Journal of Applied Mechanics and Technical Physics, Vol. 53, No. 1, pp. 98–112, 2012.

RHEOLOGY AND DYNAMICS OF REPULSIVE CLATHRATES

V. A. Eroshenko and Yu. F. Lazarev

UDC 532: 532.135: 536: 541.12: 541.18: 620.22: 621: 621.1: 62-567: 629.027

Abstract: The physical and thermodynamic properties of a repulsive clathrate used as a working body for the dissipation, storage, and conversion of energy in thermomechanical systems are studied. In repulsive clathrates, use is made for the first time of the molecular repulsive forces acting in large interfacial areas in a system consisting of a fluid and a capillary-porous matrix not wetted by this fluid. Based on experimental studies of a car damper with a repulsive clathrate, a rheological model of energy dissipation was developed which can be used to design compact high-performance dampers for different purposes and anti-seismic systems of new generation.

Keywords: suspension, interface, lyophobic interaction, compression–expansion isotherms, hysteresis, damper, experiment, simulation.

DOI: 10.1134/S0021894412010130

1. PHYSICAL AND THERMODYNAMIC PROPERTIES OF A REPULSIVE CLATHRATE

In the 1990s, it was first proposed to use interfaces in heterogeneous lyophobic systems as working fluids in thermomechanical systems [1–9]; such systems were later called repulsive clathrates [10]. In these systems, use was made of intermolecular forces of repulsion (repulsion force) and the effect of increasing surface forces, compared to body forces, with decreasing particle size, which extended the range of application of modern nanotechnologies due to the inclusion of technical thermodynamics and power engineering [1, 3–5, 11–16].

Clathrates AB ($A + B \to AB$, where A is a host molecule with the free internal space and B is a guest molecule with sizes comparable to the size of this spaces), known in chemistry [17], are formed in the case where molecule B enters the cavity of molecule A to form a chemically neutral molecule AB and does not leave it due to steric effects.

In contrast to known clathrates [17], in repulsive clathrates $A_{RC}B_{RC}$ [10], which are also chemically neutral systems, the host molecule A_{RC} is a lyophobic capillary-porous matrix with a large surface area and nanoscale voids, and the guest molecules B_{RC} are fluid molecules and clusters which are forcibly introduced into the pore space of the matrix (as a result, the volume of the repulsive clathrate $A_{RC}B_{RC}$ decreases by an amount equal to the volume of the introduced fluid). If the external pressure becomes lower than the capillary pressure, the molecules and clusters of the fluid spontaneously leave the pore space of the lyophobic matrix, because of which the volume of the clathrate $A_{RC}B_{RC}$ increases to its original value. The compression–expansion processes of the repulsive clathrate $A_{RC}B_{RC}$ become reversible along the coordinate V (volume): $A_{RC} + B_{RC} \leftrightarrow A_{RC}B_{RC}$, and the repulsive clathrate acts as a molecular spring [16].

Repulsive clathrates (Fig. 1) are suspensions consisting of a fluid and a capillary-porous powdered matrix not wetted by this fluid (contact angle at the solid–fluid interface $\theta > 90°$).

National Technical University of Ukraine "Kiev Polytechnical Institute," Kiev, 03056 Ukraine; eroshenko@kpi.ua. Translated from Prikladnaya Mekhanika i Tekhnicheskaya Fizika, Vol. 53, No. 1, pp. 114–131, January–February, 2012. Original article submitted March 11, 2011.

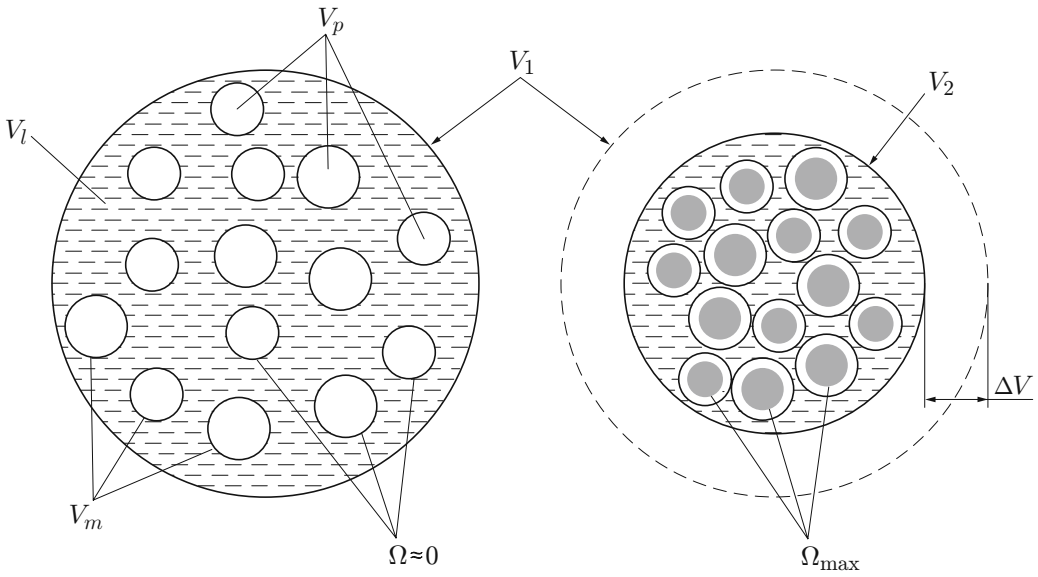

Fig. 1. Heterogeneous lyophobic system (repulsive clathrate).

The average diameter of the porous particles is 5–25 μm, and the sizes of the pores and capillaries in them are 0.5–20.0 nm. With a particle size less than 1 μm, the suspension becomes a colloid.

Because the system is lyophobic and hydrophobic, the fluid cannot spontaneously fill the open pore space of the matrix. To cause the fluid to intrude into the pore space of the matrix and produce large specific interfaces of the fluid–solid system, the external pressure should reach the threshold value equal to the Laplace capillary pressure [2, 18]

$$P_{\mathrm{L}} = 2\sigma|\cos\theta|/r. \tag{1}$$

Here σ is the surface tension of the fluid at the boundary with the gas (vacuum) and r is the radius of the pores and capillaries.

The volume V_p of the pore space of the matrix determines the degree of compression ΔV of the heterogeneous system considered (in thermodynamic studies, the elastic deformation of the fluid and the solid matrix is not considered):

$$\Delta V = V_1 - V_2 = V_p = \varphi V_m = -kr\,\Delta\Omega. \tag{2}$$

Here V_1 and V_2 [m^3] are the volumes of the system before and after compression, respectively, φ is the open porosity of the matrix with nanoscale pores and capillaries, V_m [m^3] is the volume of the matrix, $0.33 < k < 0.50$ are the shape factors of the pores and capillaries, and $\Delta\Omega$ [m^2] is the change in the area of the fluid–solid interface in the processes of forced intrusion (at a pressure P_{int}) and spontaneous extrusion (at a pressure P_{ext}) of fluid clusters from the pore space of the matrix.

Fluid extrusion is due to a spontaneous reduction in the area of the interface Ω in the lyophobic system (decrease in the Gibbs potential is equivalent to a decrease in the free surface energy of the system).

The minus sign in Eq. (2) means that during compression of the system ($\Delta V < 0$), the area of the interface increases ($\Delta\Omega > 0$), and during spontaneous expansion of the system, it decreases. From Fig. 1, it follows that the volume of the fluid V_l in the suspension should be larger than the pore space of the matrix V_p by at least an amount equal to the interparticle volume of the suspension (porosity). Since the repulsive clathrate, which is a closed system, undergoes compression and expansion, in this paper we do not consider phenomena such as the aggregate stability of a lyophobic suspension or its structuring, which have no effect on the (P–V) the compression–expansion isotherms of this heterogeneous system.

Porous matrices in the synthesis of repulsive clathrates are usually silica, aluminum silicates, porous glasses, zeolites, silicalites, and other materials with very large specific surface areas (from 100 to 1000 m^2/g) [3–5, 9, 10, 13]. The possibility of ultrafine dispersion of the fluid (up to molecular sizes or nanosizes) using these matrices indicates

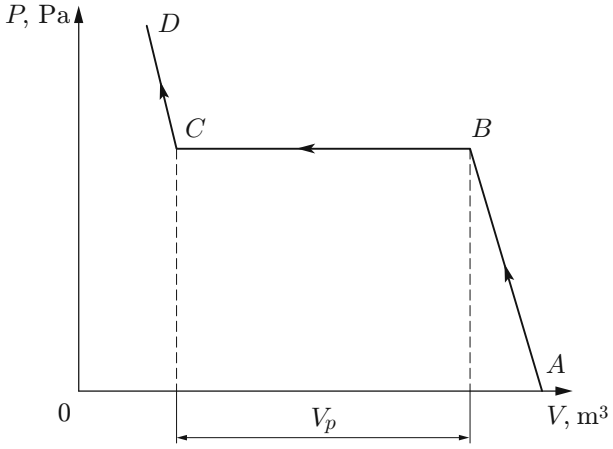

Fig. 2.

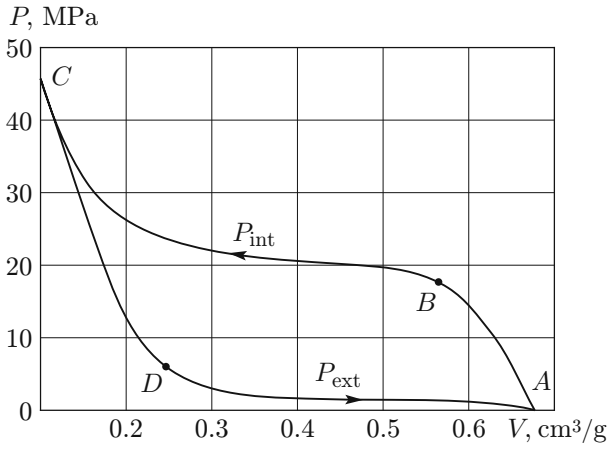

Fig. 3.

Fig. 2. $(P$–$V)$-Compression isotherm of a repulsive clathrate based on a matrix with the same pore size: AB is the region of initial elastic deformation without intrusion, BC is the region of fluid intrusion into the pore space of the matrix, and CD is the region of elastic deformation after complete filling of the pore space of the matrix with the fluid.

Fig. 3. Isothermal compression–expansion cycle of a repulsive clathrate based on a matrix with varying pore size: AB is the region of initial elastic compression without the intrusion, BC is the region of fluid intrusion into the pore space, CD is the region of spontaneous elastic expansion of the repulsive clathrate, DA is the region of spontaneous extrusion.

that the behavior of heterogeneous nanosystems is determined mainly by their surface properties and processes, and to a lesser degree by the bulk properties of the components of these systems—fluid and solid (matrix) [2, 3–5, 19]. Water and aqueous solutions, salts, and melts, low-temperature alloys, eutectic, and other simple fluids are used [3–5, 9, 10, 13].

The most important characteristic of these heterogeneous systems is their pronounced lyophobic propoerties $(120^\circ < \theta \leqslant 180^\circ)$. If a system is initially lyophilic (the fluid spontaneously enters the pore space of the matrix), it is not workable. However, the system can be made functionally suitable by chemically modifying the surface of the matrix, i.e., making it hydrophobic (nonwettable) [20].

In the case of simple fluids, the relationship between the surface tension σ and temperature T can be considered linear [2, 14]:

$$\sigma = \sigma_0(1 - T/T_*) \tag{3}$$

(T_* is the critical temperature at which $\sigma = 0$; $d\sigma/dT = -\sigma_0/T_*$ is the temperature coefficient of surface tension of the fluid).

In contrast to conventional working fluids (gas or steam), whose properties are uniquely determined by the ideal gas equation of state $PV = nRT$ or the Van der Waals equation for real gases, the properties of repulsive clathrates are determined by two independent equations:

$$dV = -kr\,d\Omega, \qquad dP = \frac{2|\cos\theta|}{r}\,\frac{d\sigma}{dT}\,dT. \tag{4}$$

Thus, it was first possible to break the relation between the conjugate parameters P and V [2, 6]. This feature of repulsive clathrates allowed them to be used to produce more advanced energy devices and systems (clean with minimal consumptions of energy and materials) and even to implement previously impossible modes of their operation [1, 3–5, 9, 13]. For example, contrary to traditional concepts, increasing the temperature in system (4) leads to a pressure drop since $d\sigma/dT < 0$ [18, 21].

Figure 2 shows a $(P$–$V)$-isotherm for a repulsive clathrate based on a matrix with the same pore size (e.g., zeolite with $r = \text{const}$) [15, 16]. It is seen that in the region AB, an increase in pressure does not lead to a substantial reduction in the volume of the quasi-condensed suspension, but after reaching a value equal to the Laplace capillary

pressure (1), fluid intrusion into the pore space of the matrix occurs in the region BC and, as a consequence, resulting in a decrease in the volume of the system as a whole (by an amount equal to the pore volume V_p). The area of the interface Ω becomes maximal at the end of the compression process (point C in Fig. 2) [see Eqs. (2) and (4)]. An increase in the pressure in the region CD after the final filling of the pores and capillaries does not lead to a substantial decrease in the volume of the system (it becomes almost incompressible again).

The isothermal compression–expansion cycle of the repulsive clathrate based on a matrix with varying pore size (r is a variable) is shown in Fig. 3 (hydrophobic silica–water system [22, 23]). It is evident that after reaching a value equal to the Laplace capillary pressure (point B), the fluid is forced to fill first large and then small pores and capillaries at a variable pressure P_{int} (region BC, in which slight elastic compression of the repulsive clathrate occurs after filling of the pore space). In the region CD, the volume components of the system undergo a slight elastic expansion and the pressure decreases, and in the region DA, the fluid clusters are spontaneously extruded from the pore space at a variable pressure P_{ext}, with the fluid first extruded from small pores and then from large ones. From Fig. 3, it follows that under cyclic loading of the repulsive clathrate, the deformation of the suspension, which is small in the regions AB and CD, becomes significant in the regions of intrusion (region BC) and extrusion (region DA) of the fluid: the volume of pore space of the matrix V_p determines most of the deformation of the system.

The cycle considered can be characterized by a large hysteresis $H = P_{\text{int}} - P_{\text{ext}}$. Clathrates with such hysteresis are used for the effective dissipation of mechanical energy (bumpers, dampers, etc.) [13, 22, 23]. Repulsive clathrates with a small hysteresis H are used to store mechanical energy [9, 15, 16].

Repulsive clathrates have a unique property that their dynamic characteristics in the pressure–volume coordinates over a wide range of frequencies can almost coincide with their (P–V)-isotherm, which is essentially a static characteristic of heterogeneous systems (a quasistatic characteristic of one of real clathrate is shown in Fig. 3).

The internal surface energy U_Ω of a repulsive clathrate (ignoring its volumetric component and, hence, the bulk internal energy of the system) can be expressed as [2, 6]

$$dU_\Omega = dW_\Omega + dQ_\Omega, \tag{5}$$

where dW_Ω is the work expended in the isothermal formation of the interfacial surface Ω and dQ_Ω is the heat expended in the isothermal formation of the surface Ω.

It should be kept in mind that

$$dW_\Omega = \sigma|\cos\theta|\,d\Omega, \qquad dQ = -T\,\frac{d\sigma}{dT}\,|\cos\theta|\,d\Omega \tag{6}$$

(see [8, 12, 24]).

From equalities (5) and (6), it follows that the isothermal compression of a repulsive clathrate (an increase in the surface area: $d\Omega > 0$) is endothermic [18]: it is required to deliver not only work to the system, but also heat necessary for the formation of the surface since $d\sigma/dT < 0$. Isothermal expansion of a heterogeneous system (spontaneous reduction in the surface area: $d\Omega < 0$) is accompanied by heat release (exothermic process) [14, 18, 19, 24]. Such phenomena are not encountered in traditional engineering thermodynamics.

2. DAMPER BASED ON A REPULSIVE CLATHRATE

A real damper of a new class [13, 22, 23] and the principle of its operation are shown schematically in Fig. 4. In a cylinder *1* filled with a small amount of a technical fluid *2* (e.g., oil), there is a piston *3* with a rod *4* (the diameter of the rod is not considered). The piston divides the cylinder into two working chambers *5* and *6*, each of which contains repulsive clathrates *7* and *8* which are placed in flexible capsules to prevent contact of the suspension with the technical fluid. Thus, clathrates *7* and *8* are arranged opposite to the piston. The compensation chamber *9* with a flexible membrane, acted upon by atmospheric pressure P_a, is connected with the working chambers *5* and *6* through bypasses based on throttles *10* and *11* and check valves *12* and *13*. An external perturbation F_A (for example, harmonic deformation $x = x_m \sin\omega t$) is applied to the rod.

The hydraulic resistance of throttles *10* and *11* increases with increasing degree of throttling α and flow velocity of the technical fluidm which is proportional to the piston velocity $\dot{x}$: $P_{\text{res}} = P_{\text{res}}(\alpha, \dot{x})$. In Fig. 5, it is

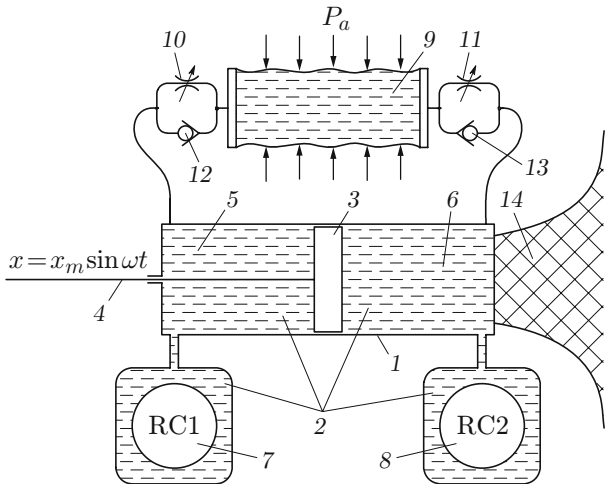

Fig. 4.

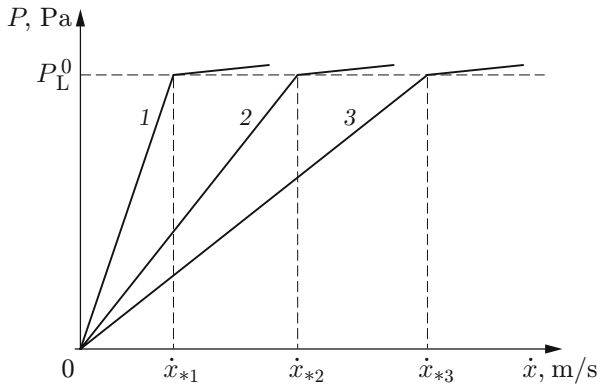

Fig. 5.

Fig. 4. Diagram of a car damper with a repulsive clathrate as a dissipating medium: (*1*) cylinder; (*2*) technical fluid; (*3*) piston; (*4*) rod; (*5, 6*) working chambers; (*7, 8*) repulsive clathrates; (*9*) compensation chamber; (*10, 11*) throttles; (*12, 13*) check valves; (*14*) protected object.

Fig. 5. Hydraulic resistance P of a throttle versus the velocity of movement $\dot{x}$ of the damper rod for $\alpha = \alpha_1$ (*1*), α_2 (*2*), and α_3 (*3*).

shown that the velocity $\dot{x}$ at which a given pressure level (for example, $P = P_{\mathrm{L}}$) is reached is the lower the greater the degree of flow throttling α ($\dot{x}_{*1} < \dot{x}_{*2} < \dot{x}_{*3}$ at $\alpha_1 > \alpha_2 > \alpha_3$).

The damper uses clathrates with a large hysteresis H for the parameter P in the compression–expansion cycle of the heterogeneous system (see Fig. 3). By selecting appropriate capillary-porous matrices with different pore size distributions and by varying the surface tension of the working fluid, it is possible to change the angle of inclination of the characteristics $P_{\mathrm{int}} - V$ and $P_{\mathrm{ext}} - V$.

The damper operates as follows. For example, the piston (see Fig. 4) moves to the right, and valve *13* is closed. If the velocity of the piston $0 < \dot{x} < \dot{x}_*$, i.e., if it does not exceed a specified value, the hydraulic pressure $P = P_{\mathrm{res}} < P_{\mathrm{L}}$ in chamber *6* cannot ensure the fluid intrusion into the pore space of the matrix but throttle *11* does not prevent overflow of the technical fluid (displaced from chamber *6*) into compensation chamber *9* and then through check valve *12* into chamber *5*. For a car damper, as a rule, $\dot{x}_* \approx 0.1\dot{x}_{\max}$, and $\dot{x}_{\max} = 1$ m/s for touring cars. In the region of low velocities $\dot{x}$, the energy is dissipated due to the viscous friction of the technical fluid.

If $\dot{x} \geqslant \dot{x}_*$, the hydraulic resistance P_{res} of throttle *11* (at a constant degree of throttling α) increases and the pressure in chamber *6* increases to $P_{\mathrm{res}} = P_{\mathrm{L}}$ (1), which is responsible for fluid intrusion into the matrix of the repulsive clathrate *8*, whose volume significantly decreases in this case. If the repulsive clathrate *7* was previously compressed, then as the piston moves to the right, the clathrate will be expanded, compensating for the deficit of the fluid volume in chamber *5*. If necessary, the fluid from compensation chamber *9* will flow into chamber *5* through valve *12* (under the action of the difference between the pressure P_a and the decompression in chamber *5*).

Similar phenomena occur when the piston moves to the left: at velocities $\dot{x} \geqslant \dot{x}_*$, forced intrusion of the working fluid into the pore space of the matrix and a significant decrease in the volume will occur in clathrate *7*, and spontaneous extrusion of fluid clusters from the pore space will occur in clathrate *8*. In this case, the opening of valve *13* will provide a supply of the required amount of the technical fluid into chamber *6* and eliminate rarefaction in the space behind the throttle (discontinuity of the fluid).

Thus, for any movement of the piston, continuity of the fluid in chambers *5* and *6* is guaranteed. In the opposite layout of repulsive clathrates *7* and *8* relative to the piston, even unilateral displacement of the latter in any direction is accompanied by complete closure of the compression–expansion cycle of the repulsive clathrate. The energy dissipated in this case is proportional to the area enclosed between the intrusion and extrusion curves in the (P–V)-diagram (see Fig. 3).

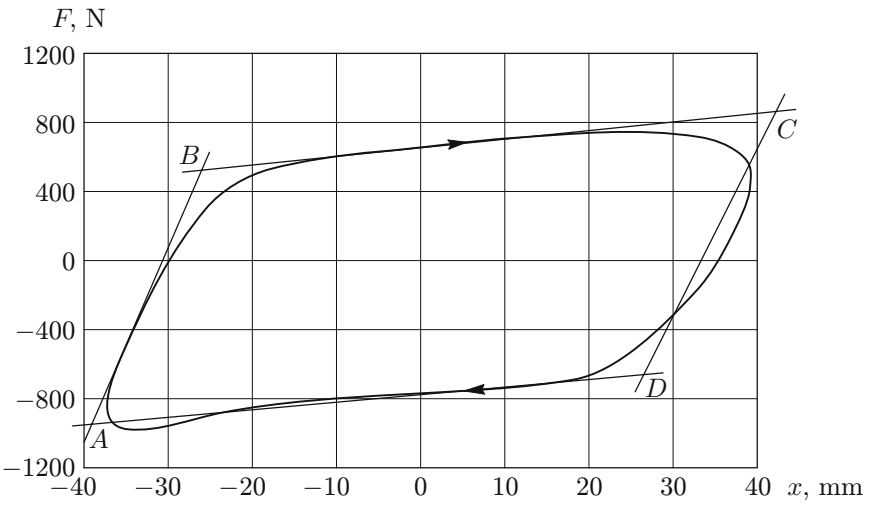

Fig. 6. Force–displacement characteristic for cyclic loading of a real damper: $ABCD$ is an approximation of the real characteristics of cyclic loading (AB and CD are the regions of elastic expansion of one of the two repulsive clathrates and the initial elastic compression of another repulsive clathrate connected oppositely and BC and DA are the regions of extrusion of the fluid in one of the two repulsive clathrates and intrusion in another repulsive clathrate).

The a damper considered can be classified as a device based on a symbiosis of two types of dissipation of mechanical energy [13, 22, 23]. On the one hand, use is made of the traditional pumping of a viscous fluid through throttles *10* and *11* (see Fig. 4) in the case of low velocities of the working body of the damper ($0 < \dot{x} < \dot{x}_*$), which results in small forces F_A on the rod. On the other hand, use is made of a fundamentally new method of energy dissipation at considerable velocities of the rod ($\dot{x} \geqslant \dot{x}_*$) [13, 22, 23] which is based on the phenomenon of a large pressure hysteresis H with increasing and decreasing area of the interfaces (compression–expansion of the repulsive clathrate). In this case, great forces F_A are not directly related to the velocity, but are determined by the large pressure drop on the piston ($H = P_{\text{int}} - P_{\text{ext}}$) during intrusion and extrusion in the heterogeneous system. This allows a significant reduction in the effective area of the working bodies (pistons) in real hydromechanical devices [3–5, 9, 13, 22, 23].

From Figs. 2 and 3, it follows that the effect of change in the area of the working fluid–matrix interfaces Ω on energy dissipation is more significant than the effect of the viscosity of the technical fluid in the traditional devices. The combination of the two types of energy dissipation in one damper allows one to speak of a generalized dissipative medium and, consequently, its generalized rheological model (see Section 3).

Figure 6 shows the force–displacement characteristic of a real damper [13, 23] (at a loading frequency equal to 1 Hz), which is a consequence of individual characteristics (see Fig. 3) of repulsive clathrates *7* and *8* in Fig. 4. A detailed description of the method of experimental determination of the dynamic properties of the new damper is given in [22, 23].

Repulsive clathrates *7* and *8* (see Fig. 4) are connected hydraulically oppositely relative to the piston, so that if in one of the working chambers (*5* and *7* or *6* and *8*), the heterogeneous working medium is compressed ($dV < 0$, $d\Omega > 0$), then, in the other chamber, it is expanded ($dV > 0$, $d\Omega < 0$). Since the nominal position of the piston (the origin along the x direction) is taken to be its position in the middle of the cylindrical part *1* of the damper (see Fig. 4), the forces F_A on the rod change sign depending on the sign of the displacement x (see Fig. 6).

3. GENERALIZED RHEOLOGICAL MODEL OF A DISSIPATIVE MEDIUM BASED ON A REPULSIVE CLATHRATE

In the case of a lyophobic suspension, the laws of continuum mechanics can be used. Despite the great variety of existing rheological models [25, 26], none of them is suitable for a correct description of the rheological properties of the repulsive clathrate.

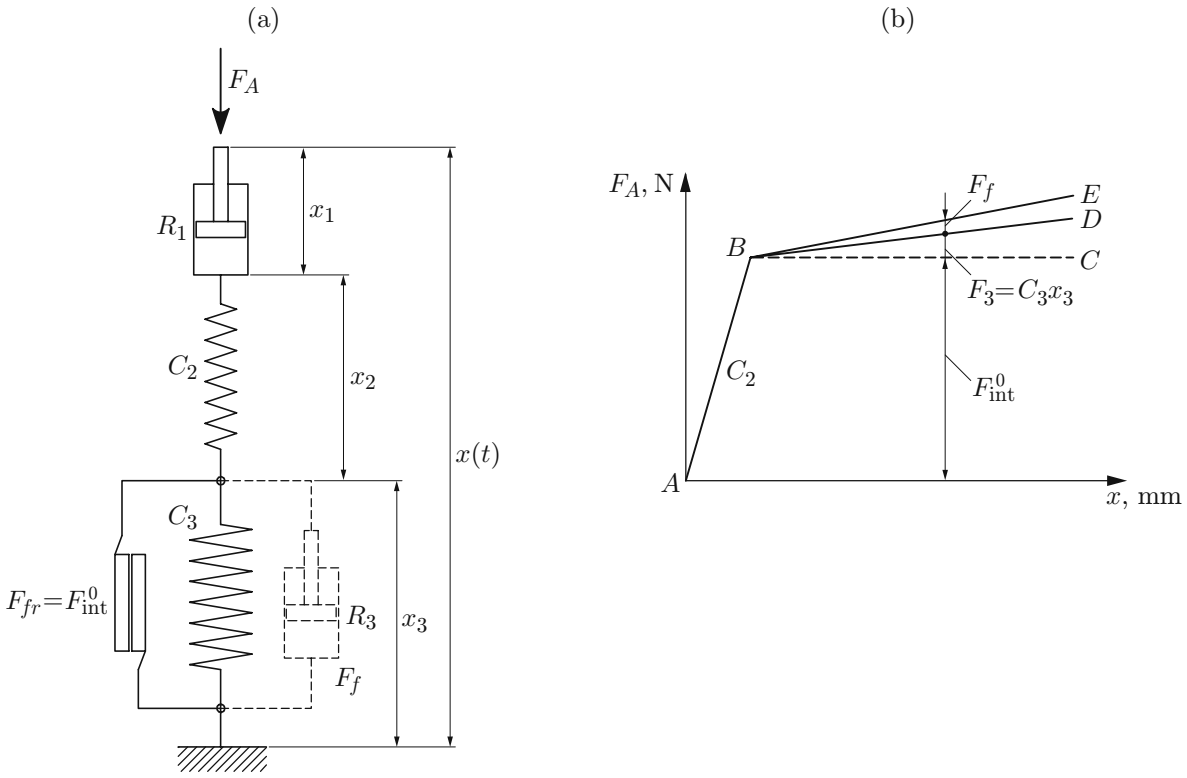

Fig. 7. Generalized rheological model of a repulsive clathrate: (a) diagram and element base of the model; (b) force F_A versus displacement of the rod x (AB for elastic deformation of the repulsive clathrate, BC for fluid intrusion for a repulsive clathrate based on a matrix with the same pore size, BD for fluid intrusion for a repulsive clathrate based on a matrix with varying pore size, and BE for fluid intrusion taking into account viscous forces at ultrahigh velocities of the rod).

Figure 7a shows a diagram and element base of the proposed generalized rheological model of the working medium using a repulsive clathrate, and Fig. 7b shows the operating characteristic of the model force F_A displacement of the rod x.

The generalized model consists of a throttle and repulsive clathrate connected in series. The throttle in which there is viscous friction of the fluid, corresponds to the element R_1 with deformation x_1. Actually, the repulsive clathrate is simulated by an elastic element C_2 with deformation x_2 connected in series to a block of parallel-connected elements with displacement x_3. This block simulates the fluid intrusion and extrusion into the pore space of the matrix (see Fig. 3) and consists of the following elements: a dry friction element with force $F_{fr} = F^0_{\text{int}}$, an elastic element with stiffness C_3, and a phantom element with force F_f [the last element operates only in the high-frequency region; for details see below]. Note that in Fig. 7, $R = dF/d\dot{x}$ and $C = dF/dx$ are the damping coefficient and the elastic coefficient, respectively.

It is assumed that the displacement of $x(t)$ of the first element with respect to the fixed end of the three-link block is a given function of time. The relationship between the strains and the rates of their change is defined by the equalities

$$x(t) = x_1 + x_2 + x_3, \qquad v(t) = \dot{x}(t) = \dot{x}_1 + \dot{x}_2 + \dot{x}_3. \tag{7}$$

From the generalized rheological model of the working medium based on a repulsive clathrate (see Fig. 7a), it follows that the expression for the force F_A can be written in three ways ($F_A = F_1 = F_2 = F_3$):

$$F_A = R_1\dot{x}_1 = C_2x_2 = F_{fr} + C_3x_3 + F_f. \tag{8}$$

As noted above, the specifics of the new working body leads to an unusual graphical representation of the rheological model based on a repulsive clathrate (see Fig. 7) over a wide range of amplitudes of the velocities $v_{3m} = \omega x_{3m}$ (x_{3m} is the amplitude of displacement x_3 and $\omega = 2\pi f$ is the angular frequency as a function of the

frequency f), the force F_A is almost independent of the velocity $\dot{x}_3$, so that the force–displacement x_3 characteristic remains unchanged (line ABD in Fig. 7b). This phenomenon was observed experimentally and is apparently due to the fact that, because of nonwettability, the fluid velocity in pores and capillaries on the interface with the solid surface of the matrix has a finite value (an immovable Prandtl layer is absent). In this case, in the balance of the forces determining the fluid velocity distribution, viscous forces are of secondary importance, i.e., they have a lesser effect on the motion of the fluid in lyophobic pores and capillaries [18].

Only for $\dot{x} \geqslant \dot{x}_{mf} \approx 3$–$4$ m/s, the change in the force F_A as a function of the displacement x (i.e., the volume of the fluid intruded into the matrix) begins to be determined by the region BE in Fig. 7b (this phenomenon was also observed experimentally). Before explaining the essence of this unusual phenomenon, let us return to the interpretation of the basic characteristic ABD of the generalized rheological model (see Fig. 7b) and its relationship to the element base (see Fig. 7a).

In the region of elastic deformation (region AB), the strain x_2 of the spring C_2 is proportional to the force F_A, which depends on the displacement velocity $\dot{x}_1$: $F_A = R_1\dot{x}_1$. In turn, the force in the spring C_2 can increase to the value $F_A = F^0_{\text{int}}$ (point B in Fig. 7b) and provide a hydraulic pressure equal to the Laplace capillary pressure (1) at which the fluid can be intruded into the pore space of the matrix. If a matrix with the same pore size is used: $r = \text{const}$), the strain x_3 of the repulsive clathrate is determined by the region BC, which is characteristic of dry friction elements: $F_{fr} = F_{\text{int}}$. If a matrix with varying pore size is used ($r_{\min} < r < r_{\max}$), the deformation in the repulsive clathrate after the start of intrusion for F^0_{int} will be characterized by the region BD, i.e., by an increase in F_A because the fluid first fills pores with $r_{\max}(P_{\min})$ and then pores with $r_{\min}(P_{\max})$. The increase in the force F_A (length BD) relative to the constant value of F^0_{int} (region BC in Fig. 7b) is modeled by the spring C_3.

In dynamic tests of the damper at high velocities of the external perturbation on the repulsive clathrate ($\dot{x} \geqslant \dot{x}_{mf}$), a rare phenomenon was observed: at the same perturbation amplitudes, the variation of the forces F_A is determined by the region BE (see Fig. 7b), and the characteristic $F_A \sim x$ begins to "swell" on the coordinate F_A. Two explanation of this phenomenon can be proposed. The first explanation is based on the traditional concepts of the mechanism of dissipation of mechanical energy using the forces of viscous friction. It is believed that at high rates of interaction in the fluid–solid system, surface phenomena, in particular the effect of "slippage" of clusters in the fluid in lyophobic pores and capillaries become less significant and viscous friction in the hydraulic fluid in pores dominates, which increase with increasing velocity: $F_f = R_3\dot{x}_3$.

The second explanation, called thermodynamic, seems more realistic since it takes into account the specific properties of repulsive clathrates [2, 6, 18]. Its essence is as follows. Isothermal intrusion of the fluid into the pore space of the matrix (isothermal development of the interface Ω) is an endothermic process [18, 19]. The isothermal process of the formation of the surface Ω is provided by a balanced supply of external heat for the formation of the surface Q in according with formula (6). It is the balance between the thermal power dQ_-/dt (proportional to the rate of formation of the surface $d\Omega/dt$) necessary for the formation of the interface and the power supplied from the outside dQ_+/dt that provides constancy of the temperature as the area of the interface Ω increases. Due to the inertia of the heat transfer processes in the system of a repulsive clathrate and the ambient medium, this balance is the more reliable the lower the rate of formation of the surface $d\Omega/dt$ (the velocity of the piston is $\dot{x}$). However, with increasing velocity of the mechanical impact $\dot{x}_3$ on the repulsive clathrate starting from a certain value of $\dot{x}$, the value of dQ_-/dt increases in proportion to $d\Omega/dt$. In this process, the rate of heat supply from the outside dQ_+/dt is lower than the rate of heat consumption by the system in the process of formation of the surface. In this case, the heat exchange between the repulsive clathrate and the ambient medium is nearly adiabatic, i.e., it occurs without effective supply of heat to the system from the ambient medium. As a result, the system experiences a heat deficit, which can be compensated by a reduction in the internal energy $dU = C_V\,dT$ (C_V is the total heat capacity of the suspension at constant volume), resulting in a reduction in the temperature repulsive clathrate ($dT < 0$) [18]. This increases the surface tension of the fluid and the Laplace capillary pressure [see Eqs. (3) and (4)]. As the temperature decreases, the force F_A in the damper increases; the characteristic $F_A \sim x$ begins to "swell" (region BE in Fig. 7b) relative to the region BD. Similar phenomena are observed during extrusion, but the signs of the energy change to the opposite.

However, because $P_{\text{int}} \gg P_{\text{ext}}$ and the repulsive clathrates *7* and *8* (see Fig. 4) are switched hydraulically opposite to the piston, the thermal effects occurring during compression of the clathrate ($d\Omega > 0$) dominate over those during its expansion ($d\Omega < 0$). Thus, the compression–expansion of each clathrate *7* and *8* separately results

in an adiabatic decrease in their temperature (which is confirmed experimentally [18, 23]) and, as a consequence, in an increase in the force F_A. In spite of the validity of the thermodynamic explanation, the description of the "swelling" of the characteristic $F_A \sim x$ at high rates of change of the external perturbation F_A in rheological terms seems unnecessarily cumbersome compared to the description obtained by using the simpler traditional explanation ($F_f = R_3\dot{x}_3$). Therefore, in the further modeling and studying the dynamics of repulsive clathrate, we will use the simpler element $F_f = R_3\dot{x}_3$ in their rheological model, assuming that the aforementioned increase in the adiabatic force F_A is equivalent to the force F_f and both forces ultimately provide the same energy dissipation.

4. EXPERIMENTS AND MODELING OF THE BEHAVIOR OF REPULSIVE CLATHRATES

Repulsive clathrates were used to develop dampers for Renault Safran touring car [22, 23]. Measured forces F_A and strains x for this damper under cyclic loading (see Fig. 4) for various values of the amplitude and frequencies are shown in Figs. 8a and 8b.

The simulation was performed by numerical integration of the system of differential equations

$$F_{ne} = F_A - C_3 x_3; \tag{9}$$

$$\frac{dx_3}{dt} = \begin{cases} 0, & F_{ne} < F_{fr}, \\ (F_{ne} - F_{fr}\,\mathrm{sign}\,(F_{ne}))/R_3, & F_{ne} \geqslant F_{fr}; \end{cases} \tag{10}$$

$$\frac{dF_A}{dt} = C_2\Big(\dot{x}(t) - \dot{x}_3 - \frac{F_A}{R_1}\Big) \tag{11}$$

with respect to two variables—the total force F_A in the series-connected elements [see formula (8)] and strains x_3 of a three-link block (see Fig. 7). In system (9)–(11), F_{ne} is the external inelastic force acting on the inelastic elements in the three-link block [dry (F_{fr}) and viscous (F_f) friction elements] which can change sign during cyclic deformation; $\dot{x}(t)$ is the rate of change in the total strain, defined as a harmonic function of time $x(t) = x_m \sin\omega t$. Equation (11) was obtained from the obvious equation $\dot{F}_A = C_2\dot{x}_2$ (8) taking into account that $\dot{x}_2 = \dot{x}(t) - \dot{x}_1 - \dot{x}_3$ in view of (7), where $\dot{x}_1 = F_A/R_1$.

The basic values of the constant coefficients of the rheological model (see Fig. 7) R_1, R_3, C_2, C_3, F_{fr} were obtained from experimental results. In particular, for a series of experiments [23] whose results are presented in Figs. 6 and 8, the value of R_1 was determined using a method which follows from the graphic constructions given in Fig. 5: for a critical velocity $\dot{x}_* \approx 0.09$ m/s specified by the designers, the degree of throttling α and, consequently, the hydraulic resistance P_{res} were varied using throttles *10* and *11* (see Fig. 4) until the equality $P_{\text{res}} \approx P^0_{\text{L}} = P^0_{\text{int}}$ (the beginning of intrusion) was satisfied and the value $F^0_{\text{int}} = \Delta F = P_{\text{res}}s$ (s is the effective area of the piston) was reached. The presence of a kink near the critical velocity in the force F–velocity $\dot{x}$ characteristic (see Fig. 5) is evidence for the beginning of intrusion of the working fluid into the pore space of the matrix of the repulsive clathrate at a given velocity $\dot{x}_*$ and the basis for the calculation of R_1 by the formula $R_1 = \Delta F/\dot{x}_*$ (where $\Delta F = F^0_{\text{int}} = (960 + 540)/2 = 750$ N). The value $\Delta F = 750$ N was obtained as the mean amplitude of the force during compression (region AB in Fig. 6). Because $\dot{x}_* \approx 0.09$ m/s $= 90$ mm/s, it follows that the basic value $R_1 = 8.3$ N$\cdot$s/mm.

Estimated basic parameters of the links of the model can be determined using the quasistatic characteristic of the damper (the frequency of cyclic loading is 1 Hz) presented in Fig. 6 by constructing a parallelogram using the tangents AB (CD) and BC (AD) to the flat parts of the characteristic. The angle of slope of the sides of the parallelogram determines the stiffness $C_2 \approx 89$ N/mm of the second link, and the slope of its major sides determines the stiffness $C_3 \approx 5.0$ N/mm of the three-link block. Halves of the regions AB and CD determine the force $F_{fr} = 750$ N of dry friction in the three-link block.

The calculation results the closest to the experimental values (see Figs. 8a and 8b) were obtained for the following parameters of the model: $R_1 = 8$ N$\cdot$s/mm, $R_3 = 0.005$ N$\cdot$s/mm, $C_2 = 89$ N/mm, $C_3 = 6$ N/mm, $F_{fr} = 750$ N (see Figs. 8c and 8d). The low damping coefficient R_3 (for $\dot{x} \leqslant 2$ m/s, it can be ignored) confirms the assumption that the phantom link F_f (see Fig. 7) works only at velocities of movement of the piston rod of the damper (3–4 m/s).

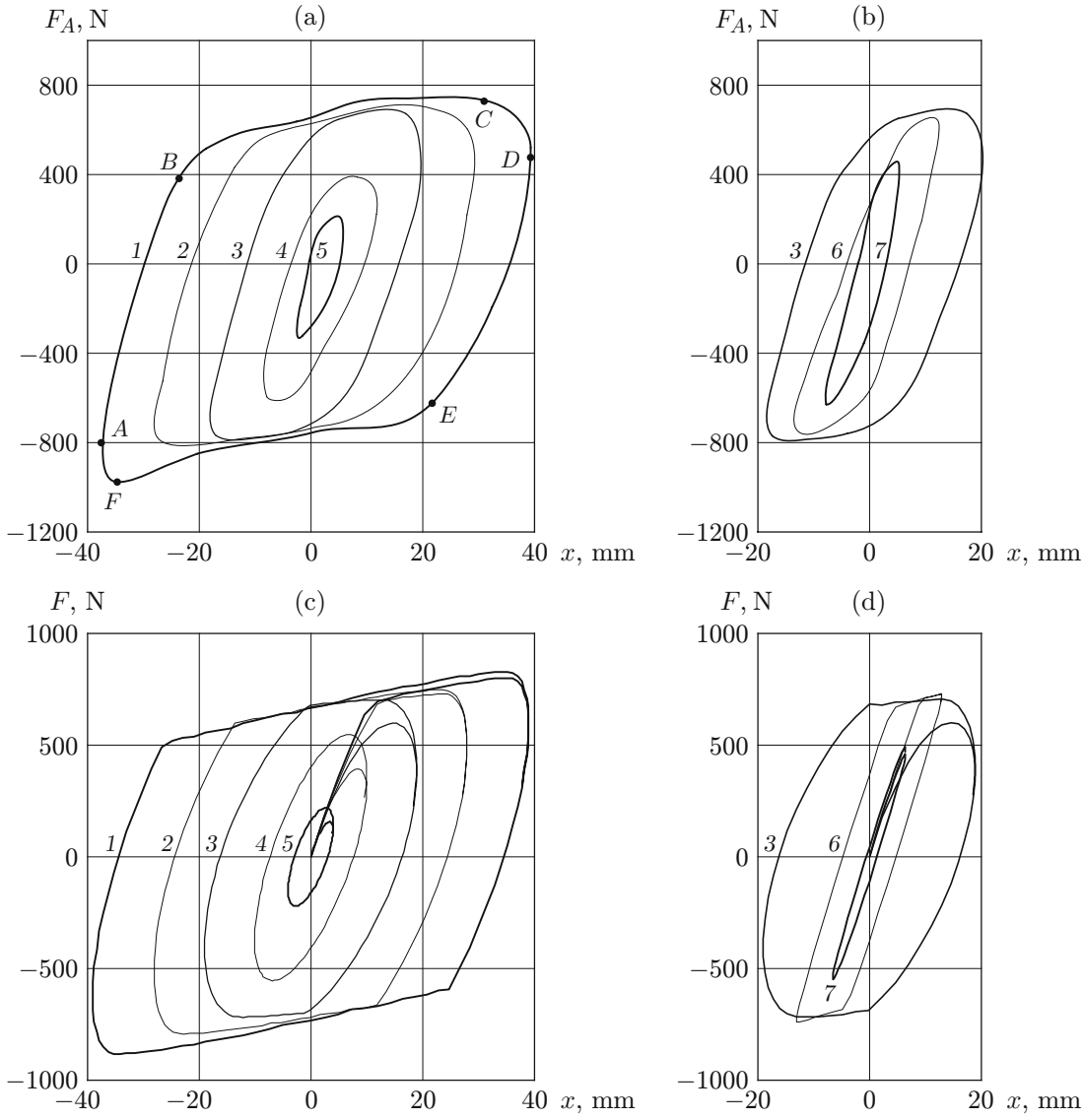

Fig. 8. Loading curves of the damper during cyclic deformation (see Table 1), obtained in experiments (a and b) and simulations (c and d): AB and DE are the regions of elastic compression of the repulsive clathrate in one of the two oppositely switched working chambers and the expansion in the other chamber; BC, and EF are the regions of fluid intrusion into the pore space of the repulsive clathrate in one of two chambers and extrusion of the fluid into the other chamber.

Table 1

Figure 8	Curve	x_m, mm	f, Hz	$\dot{x}$, m/s
(a), (c)	*1*	40	1.0	0.251
(a), (c)	*2*	30	1.0	0.188
(a)–(d)	*3*	20	1.0	0.126
(a), (c)	*4*	10	1.5	0.094
(a), (c)	*5*	5	1.5	0.047
(b), (d)	*6*	13	12.0	0.754
(b), (d)	*7*	6.5	12.0	0.377

The initial conditions for system (9)–(11) corresponded to the undeformed unloaded state of the working bodies (the piston of the damper was in the neutral position, i.e., in the central part of the cylinder 1 in Fig. 4). Therefore, the simulated loading curves start at the origin (see Figs. 8c and 8d).

The contours *3–5* given in Figs. 8a and 8b show that under harmonic loading of the repulsive clathrate, the main factor of fluid intrusion and extrusion into the pore space of the matrix is the linear velocity of the fluid $v_{3m} = \omega x_{3m} = 2\pi f x_{3m}$. It is seen that for small amplitudes ($x_m = 5$ and 10 mm) and low frequencies ($f = 1$ Hz) and, consequently, at velocities lower than the critical one $\dot{x}_*$ (see Fig. 5), the working fluid does not enter the pore space of the matrix because the pressure in the system is below the Laplace capillary pressure (see Fig. 8a). Nevertheless, at high frequencies ($f = 12$ Hz), the fluid enters the pores (see Fig. 8b) since at high velocities of the piston in the working chamber (*5* and *6* in Fig. 4), increasing P_{res} leads to the establishment of the Laplace capillary pressure (1), i.e., the intrusion pressure.

Effective energy dissipation in the cycle of increasing–decreasing surface area Ω is achieved due to the fact that the pressure of fluid extrusion from the pore space is an order of magnitude lower than the intrusion pressure (hysteresis H). This is most clearly seen when comparing the contours *4* and *6* in Figs. 8a and 8b ($x_m \approx 10$ mm): the area covered by contour *6* in Fig. 8b is larger than the area covered by the contour *4* in Fig. 8a. A similar pattern is observed for contour *5* ($x_m = 5$mm). The dissipated energy (area covered by contour *7* in Fig. 8b) increases with increasing perturbation frequency.

A comparison of the results of the experiment and simulation shows that the proposed rheological model (see Fig. 7) satisfactorily approximates experimental data.

A second series of experiments was carried out on test stands of the PSA (Peugeot–Citroen) automotive company, but with other settings and slightly modified geometric parameters of the damper (Figs. 9a and 9b and Figs. 10a and 10b). Results of the experiments on cyclic loading of the damper with amplitudes equal to 60 and 50 mm for various deformation frequencies are shown in Fig. 9a (velocity of the rod $\dot{x} = 0.19$–1.13 m/s) and Fig. 9b ($\dot{x} = 0.16$–0.94 m/s).

In Fig. 10, it is evident that in the series of experiments with $x_m = 30$ and 40 mm, nonlinear regions (saturation zone) were recorded in the working characteristics of the damper, in spite of its harmonic loading [$\dot{x}(t) = x_0 \sin \omega t$]. It is not ruled out that the appearance of these regions is due to the imperfection of the setting of the bypasses (throttle–check valve) *10, 12* and *11, 13* of the damper (see Fig. 4) in this series of experiments.

In the loading curves for deformation amplitudes $x_m = 30$ and 40 mm (see Figs. 10a and 10b), one can see the "swelling" effect which is manifested at elevated velocities of the rod (from 0.13 to 3.78 m/s in Fig. 10a and from 0.09 to 3.96 m/s in Fig. 10b). This made it possible to determine the basic value of the damping coefficient R_3^0 from the observed increase in the force ΔF caused by an increase in the velocity of the piston $\Delta\dot{x}$: $R_3^0 = \Delta F/\Delta\dot{x}$. In the experiments whose results are presented in Fig. 10a, the values $\Delta F = 160$ N, $\Delta\dot{x} = 3517$ mm/s, and $R_3^0 = 0.05$ N·s/mm were obtained. Similarly, for the experimental data presented in Fig. 10b, the values $\Delta F = 240$ N and $\Delta\dot{x} = 3768$ mm/s were obtained; therefore, $R_3^0 = 0.06$ N·s/mm.

The results of simulations using Eqs. (8)-(11) are in satisfactory agreement with the data of experiments carried out by the PSA firm for the following parameters of the model: $R_1 = 20$ N·s/mm, $R_3 = 0.07$ N·s/mm, $C_2 = 150$ N/mm, $C_3 = 2$ N/mm, and $F_{fr} = 850$ N. Thus, the parameter $R_3 = 0.005$ N·s/mm for the damper tested by the Renault firm is an order of magnitude smaller than the parameter $R_3 = 0.05$ N·s/mm determined from the results of tests of the slightly modified damper performed by PSA (see Figs. 9 and 10).

The best agreement between the experimental results and simulation data is observed for $x_m = 50$ and 60 mm (see Fig. 9). This is due to moderate linear velocities of the rod (piston) of the damper. For $x_m = 60$ mm, increasing the oscillation frequency increased the velocity of the rod from 0.19 to 1.13 m/s by; and for $x_m = 50$ mm, increasing the frequency of loading of the damper increased the velocity of the rod from 0.16 to 0.94 m/s (the standard range of velocities for the hydraulic dampers of cars).

Increasing the velocities of the piston rod of the damper from 0.13 to 3.78 m/s for $x_m = 40$ mm (see Fig. 10a) and from 0.09 to 3.96 m/s for $x_m = 30$ mm (see Fig. 10b) is apparently responsible for the transition from the cyclic isothermal mode of increasing–decreasing area of the interface of Ω (at high velocities of the piston) to the quasiadiabatic mode. Under these conditions, the rate of heat supply from the outside to the repulsive clathrate dQ_+/dt at velocities of the rod $\dot{x} = 3$–4 m/s became lower than the required (consumed) power dQ_-/dt due to an increase in the rate of formation of the interface $d\Omega/dt$. This caused relative cooling of the system (in an adiabatic

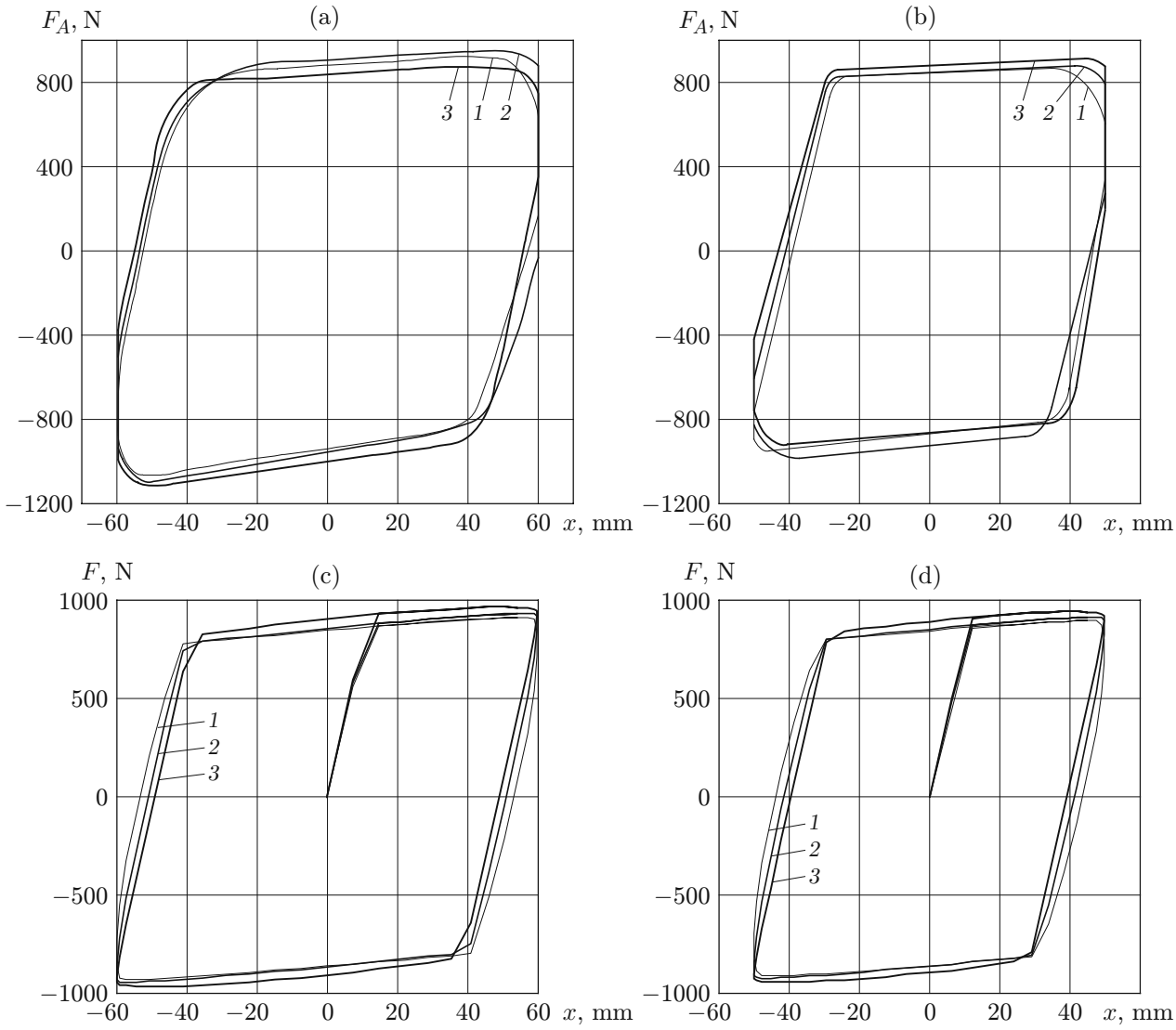

Fig. 9. Loading curves of the damper obtained in experiment (a and b) and simulation (c and d) for $x_m = 50$ and 60 mm (see Table 2).

Table 2

Figure 9	Curve	x_m, mm	f, Hz	$\dot{x}$, m/s
(a), (c)	*1*	60	0.5	0.188
	2		1.0	0.376
	3		3.0	1.130
(b), (d)	*1*	50	0.5	0.157
	2		1.0	0.314
	3		3.0	0.942

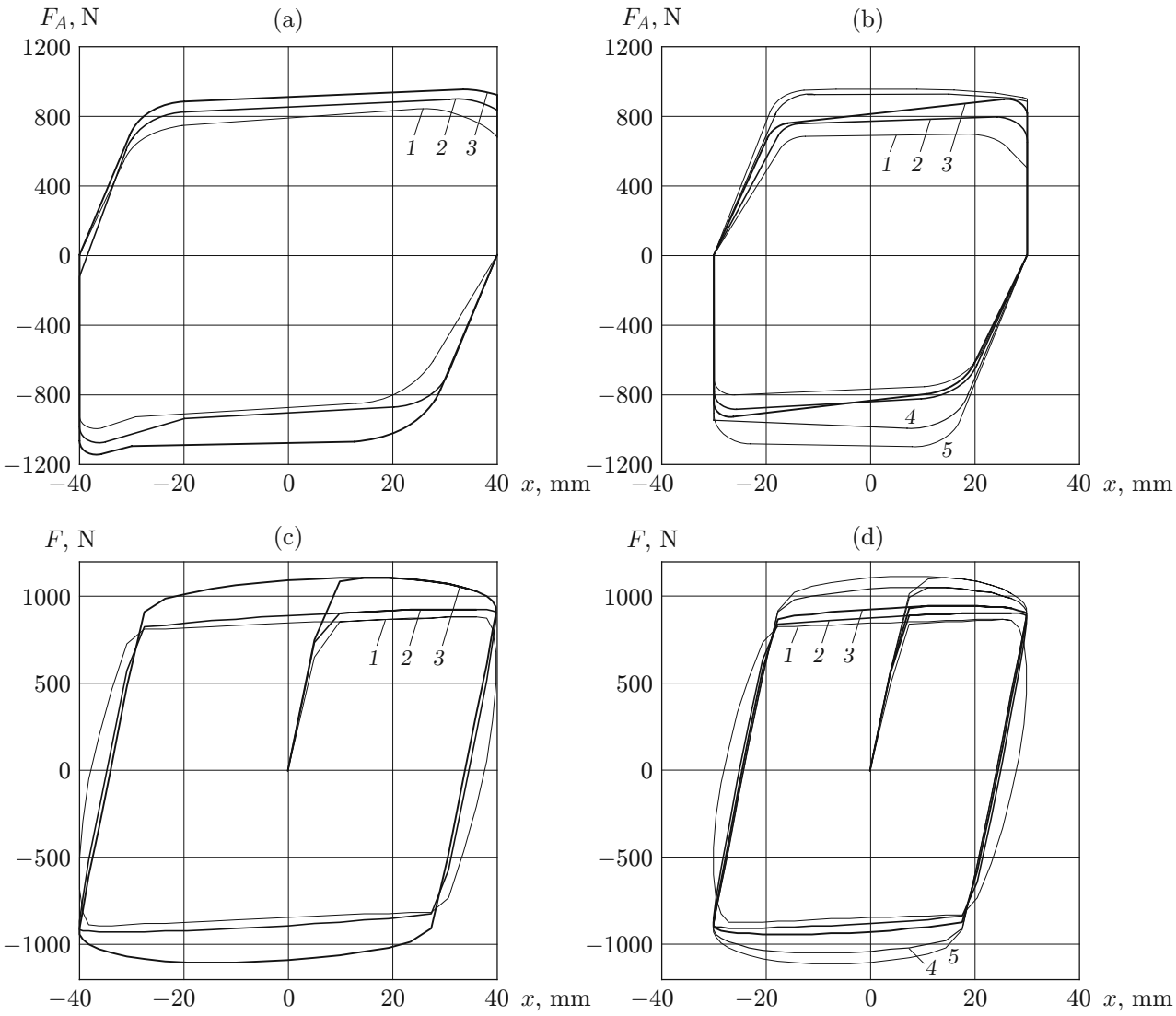

Fig. 10. Loading curves of the damper obtained in experiments (a and b) and simulations (c and d) for $x_m = 30$, 40 mm (see Table 3).

Table 3

Figure 10	Curve	x_m, mm	f, Hz	$\dot{x}$, m/s
(a), (c)	1	40	0.5	0.13
	2		3.0	0.76
	3		15.0	3.78
(b), (d)	*1*	30	0.5	0.09
	2		3.0	0.57
	3		7.0	1.32
	4		16.0	3.01
	5		21.0	3.96

process, the heat of formation of the surface is achieved by reducing the internal energy of the system, i.e., by decreasing its temperature [18]). Therefore, the pressure of fluid intrusion into the pores increases: as the piston velocity is increased, the force–displacement characteristics of the damper in Figs. 10 a and 10b "swells."

Given the complexity of the thermomechanical processes occurring in the repulsive clathrate, the model of the dynamics of the damper at high velocities (see Figs. 9c and 9d) for constant parameters of the rheological model R_1, C_2, F_{fr}, C_3, and R_3 (as in the experiments whose results are presented in Figs. 8c and 8d) can also be regarded as satisfactory.

We note that in experiments with dampers of the new class s [22, 23], effective energy dissipation was achieved even the frequencies of external mechanical perturbation on a car wheel and the velocities of the damper rod far excedded the same parameters for the hydraulic dampers of cars: at a frequency $f = 12$ Hz, the velocity of the rod was 2 m/s and at a frequency $f = 20$ Hz, it was more than 4 m/s (both of these velocities of the rod are unobtainable when using conventional hydraulic dampers). At comparable frequencies and amplitudes of loading of conventional dampers and repulsive clathrate based dampers, the specific power of energy dissipation of the latter varied from 10 to 30–40 W/cm^3 [23], which is 50–100 times higher than the same parameter for hydraulic dampers.

CONLCUSIONS

This paper described the physical principles of operation of new working bodies—repulsive clathrates in which molecular repulsion forces act in large specific interfacial areas of heterogeneous systems (suspensions) consisting of a fluid and a capillary–porous matrix not wetted by this fluid.

The thermodynamic, hydromechanic, and energy converting features of the repulsive clathrate have no analogs in modern technical thermodynamics.

A five-link generalized rheological model of a repulsive clathrate is proposed which consists of series-connected Newton and Hooke elements and a three-link block comprising parallel-connected Saint-Venant and Hooke elements and a phantom link. The five-link model of repulsive clathrates can be reduced to a three-link model consisting of a Maxwell element connected in series with parallel-connected Voigt and St. Venant elements.

Results of tests of repulsive clathrate based damper showed that the proposed equations (7)–(9) and the differential equations (10) and (11) adequately describe the rheological behavior of repulsive clathrates.

The use of repulsive clathrates in engineering provides opportunities for designing high-performance compact dissipaters of mechanical energy (dampers, bumpers, and anti-seismic and anti-vibration systems) with a wider bandwidth. In particular, vehicles equipped with high-speed dampers based on repulsive clathrates can safely overcome road obstacles without mechanical failure at velocities 2–4 times higher than the velocity of vehicles equipped with conventional hydraulic dampers.

The high efficiency of mechanical energy dissipation by repulsive clathrates is comparable to the efficiency of dissipation of mechanical energy by living coral reefs (hydrophobic heterogeneous systems) [27, 28], which are able to withstand ocean waves during storms and tsunamis.

We are grateful to F. F. Guingand and M. Zwiller from PSA Peugeot–Citroen company and L. Coiffard from Ecole Polytechnique in Paris for assistance in the experiments, as well as V. P. Stoudenets and I. I. Pyatiletov for helpful discussions of the experimental results and help in preparing the manuscript.

REFERENCES

1. V. A. Eroshenko, *Heterogeneous Thermodynamic System and Eroshenko's Method for Converting Thermal Energy into Mechanical Energy and a Device for Its Implementation*, USSR Patent No. 1,254,811 A, DSP, Appl. July 24, 1981 (1981); RF Patent No. F 03 G 7/00 (1993), Publ. September 30, 1996, Byull. No. 3.
2. V. A. Eroshenko, "Thermodynamics of Intrusion of Liquid Metals into Hard Porous Matrices," in *Capillary Properties and Adhesion of Alloys* (Naukova Dumka, Kiev, 1987), pp. 100–109 [in Russian].
3. V. A. Eroshenko, *Gidrokapillyarny Battery*, USSR Patent No. 943444 (1980), Appl. April 28, 1980, Publ. July 15, 1982, Byull. No. 26; RF Patent No. F 15 B 1/04 (1993).

4. V. A. Eroshenko, "Eroshenko's Method of Converting Thermal Energy into Mechanical," USSR Patent No. 1380357 A2, DSP (1983), Appl. November 30, 1983; RF Patent No. F 03 G 7/00 (1993), Publ. September 30, 1996, Byull. No. 3.
5. V. A. Eroshenko, "Eroshenko's Rotor Heat Engine," USSR Patent No. 1452262, DSP (1986), Appl. June 16, 1986; RF Patent No. A1 F03 G 7/00 (1993), Publ. September 30, 1996, Byull. No. 3.
6. V. A. Eroshenko, "Unusual Properties of a Complex Thermodynamic System," Dokl. Akad Nauk Ukr. SSR, Ser. A, Fiz. Mat. Tekh. Nauk, No. 10, 79–82 (1990).
7. V. A. Eroshenko, "Thermomolecular Energy," Prom. Teplotekh. **14** (1–3), 22–25 (1992).
8. V. A. Eroshenko, "Dimension of the Space As a Thermodynamic Potential of the System," Dokl. Akad Nauk Ukr., Ser. A, Fiz. Mat. Tekh. Nauk, No. 5, 65–67 (1993).
9. V. A. Eroshenko, "Heterogeneous Structure for Accumulation or Dissipation of Energy, Process to Use It and Associated Devices," FR Patent No. WO 96/18040, F 15 B 1/04, F 16 F 9/00, 5/00, F 15 B 21/06 (June 13, 1996).
10. V. A. Eroshenko, "Repulsive Clathrates. A New Operational Material for Efficient Seismic Isolation," in *Proc. of the Int. Post-SMITR Conf. "Seismic Isolation, Passive Energy Dissipation and Active Control of Seismic Vibrations of Structure," Taormina (Sicily, Italy), Aug. 25–27, 1997* (GLIS-IAEA, Roma, 1997), pp. 783–794.
11. V. A. Eroshenko and S. G. Tkachenko, "Effect of Hyperdilatometry of One Complex Thermodynamic Systems," Ukr. Fiz. Zh. **38** (12), 1789–1792 (1993).
12. V. A. Eroshenko, "Dimensionnalité de l'espace comme potentiel thermodynamique d'un système (version élargie)," Entropie **202/203**, 110–114 (1997).
13. V. A. Eroshenko, "Damper with High Dissipating Power," FR Patent No. WO 01/55616 A1, F 16 F 9/00, (August 02, 2001).
14. V. A. Eroshenko and V. P. Stoudenets, "The Influence of Developed Interfaces upon the Heterogeneous Nanosystem Thermal Capacity," Composites, Part A **33**, 1349–1353 (2002).
15. V. Eroshenko, R.-C. Regis, M. Soulard, and J. Patarin, "Energetics: A New Field of Applications for Hydrophobic Zeolites," J. Amer. Chem. Soc. **123**, 8129–8130 (2001).
16. V. Eroshenko, R.-C. Regis, M. Soulard, and J. Patarin, "Les systèmes hétérogènes "eau-zéolithe hydrophobe": de nouveaux ressorts moléculaires," C. R. Physique **3**, 111–119 (2002).
17. J.-M. Lehn, *La chimie supramoléculaire* (De Boeck et Locier, Paris, 1997).
18. V. A. Eroshenko, "Effect of Heat on the Filling of Lyophobic Pores and Capillaries with Liquid," Colloid. J. **49** (5), 875–880 (1987).
19. L. Coiffard, V. A. Eroshenko, and J.-P. Grolier, "Thermomechanics of the Movement of Interface in Heterogeneous Lyophobic Systems," AIChE J **51** (4), 1246–1257 (2005).
20. V. A. Eroshenko and A. Yu. Fadeev, "Study of Chemically Modified Silica Surface Using Water Porosimetry," Zh. Fiz. Khim. **70** (8), 1482–1486 (1996).
21. V. A. Eroshenko, "Non-compressibilité et non-dilatabilité adiabatiques d'un système thermodyna mique complexe," Entropie **196**, 17–23 (1996).
22. V. A. Eroshenko, "A New Paradigm of Mechanical Energy Dissipation. Part 1. Theoretical Aspects and Practical Solutions," in *Proc. Mech. Eng. Part: DJ Automobile Eng.* **221** (3) 285–300 (2007).
23. V. A. Eroshenko, I. I. Piatiletov, L. Coiffard, and V. P. Stoudenets, "A New Paradigm of Mechanical Energy Dissipation. Part 2. Experimental Investigation and Effectiveness of a Novel Damper," in *Proc. Mech. Eng., Part: DJ Automobile Eng.* **221** (3), 301–312 (2007).
24. L. Coiffard and V. Eroshenko, "Temperature Effect on Water Intrusion/Expulsion in Grafted Silica Gels," J. Colloid Interface Sci. **300**, 304–309 (2006).
25. M. Reiner, "Rheology," in *Handbuch der Phizik*, No. VI: *Elastizität und Plastizität* (Springer-Verlag, Berlin, 1958).
26. N. B. Uriev, *Physicochemical Fundamentals of Disperse Systems and Materials* (Khimiya, Moscow, 1988).
27. V. A. Eroshenko, *The Role of Thermodynamic and Space Factors in the Structure, Functioning, and Distribution of Coral Reefs*, Preprint (Kovalevskii Inst. of Biology of Southern Seas, Acad. of Sci. of Ukraine, Sevastopol', 1993).
28. V. A. Eroshenko, "The Role of Thermodynamic and Space Factors in the Evolution of Coral Reefs," Ros. Khim. Zh. **39** (2), 72–84 (1995).